Inward diffusion driven by low frequency fluctuations in self-organizing magnetospheric plasma

PAPER

Inward diffusion driven by low frequency fluctuations in self-organizing magnetospheric plasma

IOP Publishing | International Atomic Energy Agency Nuclear Fusion

Nucl. Fusion **62** (2022) 026041 (6pp) https://doi.org/10.1088/1741-4326/ac412c

Inward diffusion driven by low frequency fluctuations in self-organizing magnetospheric plasma

N. Kenmochi[1,*], Y. Yokota[2], M. Nishiura[1,2], H. Saitoh[2], N. Sato[2], K. Nakamura[2], T. Mori[2], K. Ueda[2] and Z. Yoshida[2]

[1] National Institute for Fusion Science, Gifu 509-5292, Japan
[2] Graduate School of Frontier Sciences, The University of Tokyo, Chiba 277-8561, Japan

E-mail: kenmochi.naoki@nifs.ac.jp

Received 25 May 2021, revised 10 November 2021
Accepted for publication 8 December 2021
Published 5 January 2022

Abstract

The new findings for dynamic process of inward diffusion in the magnetospheric plasma are reported on the Ring Trap 1 (RT-1) experiment: (i) the evolution of local density profile in the self-organized process has been analyzed by the newly developed tomographic reconstruction applying a deep learning method; (ii) the impact of neutral-gas injection excites low-frequency fluctuations, which continues until the peaked density profile recovers. The fluctuations have magnetic components (suggesting the high-beta effect) which have two different frequencies and propagation directions. The phase velocities are of the order of magnetization drifts, and both the velocities and the intensities increase in proportion to the electron density. The self-regulating mechanism of density profile works most apparently in the naturally made confinement system, magnetosphere, which teaches the basic physics of long-lived structures underlying every stationary confinement scheme.

Keywords: particle confinement, transport, dipole field, magnetosphere, deep learning, tomography

(Some figures may appear in colour only in the online journal)

1. Introduction

The Ring Trap 1 (RT-1) device is a laboratory magnetosphere that is realized by a levitated superconducting ring magnet in vacuum (see figure 1) [1, 2]. The spontaneous confinement of high-beta plasma in the magnetospheric configuration results from the inward (or uphill) diffusion driven by 'low-frequency' fluctuation; the relevant frequency must be in the ion drift frequency range so that the constancy of the angular momentum is broken, while the actions of the bounce and gyro motions are conserved. The topological constraints due to these adiabatic invariants explain the inward diffusion [3, 4]. The RT-1 device confines a high-beta plasma (local electron beta $\sim$1) in a dipole magnetic field. The density has a strongly peaked profile that is explained as the homogenization of particle number among different magnetic flux tubes. In the high-density regime of the RT-1, interferometers and a reflectometer have observed edge localized fluctuations in the electron density which has a discrete spectrum of cascade modes at a frequency less than 1 kHz [5, 6]. The fluctuation level increases obviously near the cut-off density, suggesting the density dependence of the fluctuations. The particle transport characterizes a turbulent diffusion driven by the electric-field fluctuations which are related to the presence of entropy modes observed in a laboratory magnetospheric plasma of the LDX [7, 8].

In this paper, we show the new findings for the dynamic process of inward diffusion in the magnetospheric plasma in the RT-1 experiment. In section 2, a newly developed deep learning tomographic technique was applied to detect detailed

* Author to whom any correspondence should be addressed.

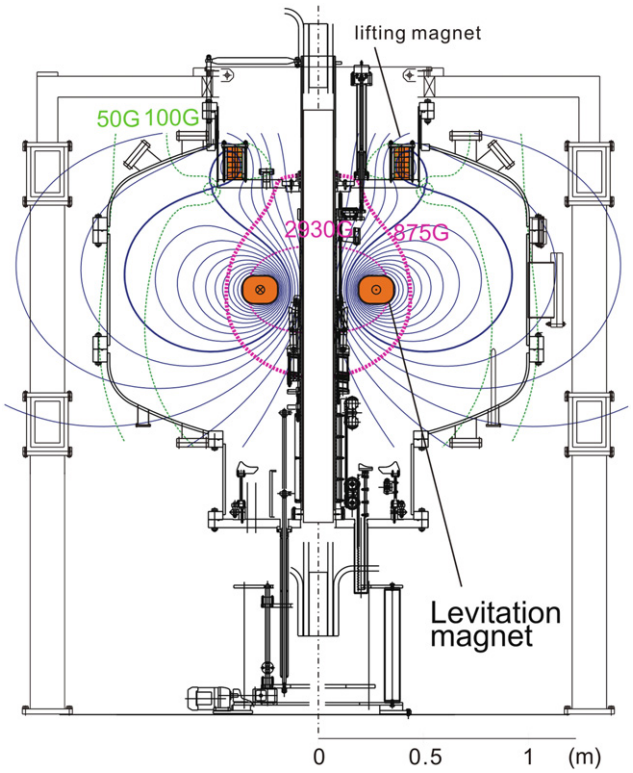

Figure 1. Cross-sectional view of RT-1.

changes in density according to the inward diffusion. The spatio-temporal characteristics of the low-frequency fluctuations associated with the inward diffusion are reported in section 3. Section 4 gives the summary.

2. Formation of self-organized plasmas

Perturbing the density profile by neutral-gas injection, we demonstrate the excitation of low-frequency fluctuations which persist until the inward diffusion reproduces the self-organized density profile [9]. In the previous study of the RT-1, the electron density profile was estimated by parameters that best fit the measured value of the line-integrated electron density by the interferometer of three lines of sight for the density profile model given by the magnetic flux surface function. In this study, the density profiles were reconstructed with less dependence on the model function by using an imaging diagnostic.

A tomographic reconstruction method using a deep learning technique has been developed to obtain local-intensity profiles from imaging-diagnostic data [10]. The pairs of local emissivity and line-integrated images which simulate an experimental system are prepared to train a network using the model function for plasma profile developed in previous studies of the RT-1 [9, 11]. After validating the accuracy of the trained network, the network reconstructs a local image from the line-integrated image measured by the imaging-diagnostics. In order to obtain local electron density profiles, this procedure has been applied to an imaging diagnostic of neutral helium emission in the RT-1 magnetospheric plasmas, including the effects of stray light within the measured image to remove reflections from the chamber walls in the reconstruction. Using a pair of emission lines of neutral helium with wavelengths of 388 nm and 447 nm, each line-of-sight integrated image measured by a high-speed camera (nac Image Technology Inc., MEMRECAM ACS-3) combining an image intensifier is reconstructed to a local-intensity profile by the tomographic method. In order to estimate the absolute value of the emission amount of each emission line from the measured image, the sensitivity of the emission amount of the optical system was calibrated using a calibration light source and an integrating sphere. The local value of the electron density is obtained by line-ratio spectroscopy by taking the ratio of these two local-intensity profiles. The absolute value of the density is calibrated using that which was measured by the interferometer. Figures 2(a) and (c) show the measured emission at 388 nm and 447 nm, respectively, which are line-of-sight integrated information. Figures 2(b) and (d) show the local-intensity profiles of emission at 388 nm and 447 nm using the tomographic reconstruction method, respectively. The ratio of the emission at 388 nm to that at 447 nm is converted to the electron density value by line-ratio spectroscopy in figure 2(f).

In order to investigate the change in the shape of the density profile due to the inward diffusion, the density profile was flattened once by the injection of neutral-gas, and then the reproduction of the peaked density profile by the inward diffusion was caused. Figures 2(e) and (f) show the local density profiles before and after the inward diffusion obtained by this method, respectively. Note that white regions in the figures indicate the areas where the emission of neutral helium is insufficient to obtain accurate density information. Comparing the figures 2(e) and (f), it is shown that the density around $z = 0$ m and $r = 0.55$ m increases due to inward diffusion. The local density profile shows that a peak density profile is formed in the high magnetic field side near the levitation coil as the result of inward diffusion. Furthermore, after the inward diffusion (figure 2(f)), the peaked density regions are distributed along the shape of the magnetic flux tube. This result is consistent with previous studies in the RT-1, and it is revealed that the density profile is sharper than the previously estimated shape.

3. Characteristics of low-frequency fluctuation with inward diffusion

Simultaneous excitation of low-frequency fluctuations during the inward diffusion are observed in electrostatic potential, electron density, and magnetic field ($B_{\parallel}$ direction) measured by a floating potential probe, interferometers, and magnetic probes, respectively. For the same purpose as in section 2, the neutral-gas is injected into the plasma in order to investigate the fluctuation characteristics associated with the inward diffusion. Figure 3(a) shows a time evolution of the spectrum of magnetic fluctuation measured by a magnetic probe. A neutral gas is injected at $t = 1.56$ s and the inward diffusion occurs until $t \sim 2.1$ s. The fluctuations of two frequency components whose frequencies are $\sim$1 kHz and $\sim$0.7 kHz are observed

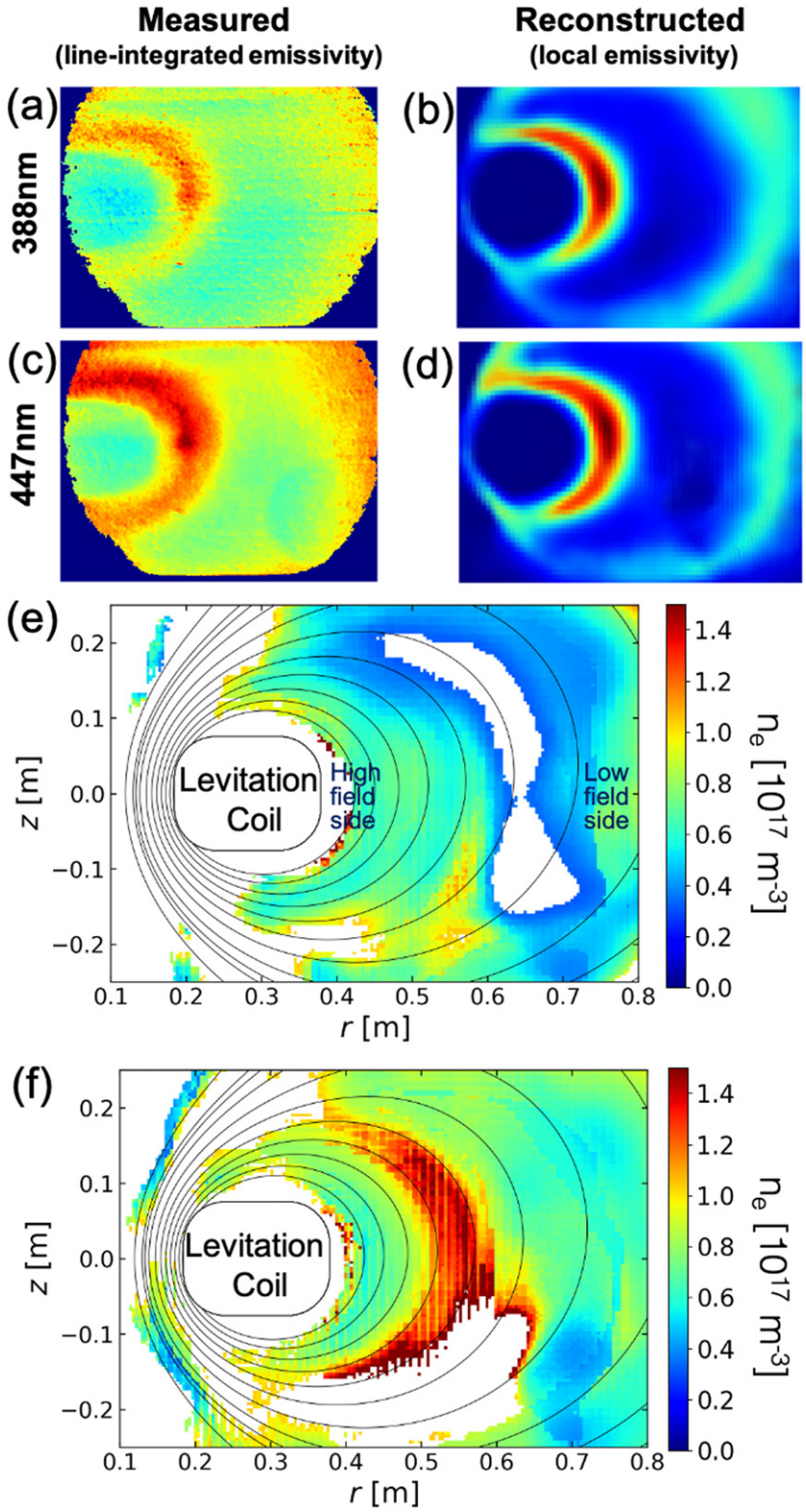

Figure 2. The line-of-sight integrals of the measured emission profiles at (*a*) 338 nm and (*c*) 447 nm. (*b*) and (*d*) are 2D images which are converted to local-emission profiles by tomography using deep learning for 338 nm and 447 nm, respectively. (*e*) and (*f*) are the local density profiles before and after the inward diffusion, respectively. The white region shows the areas where the emission of neutral helium is insufficient to obtain accurate density information. A peak density profile is formed as the result of inward diffusion (see (*f*)).

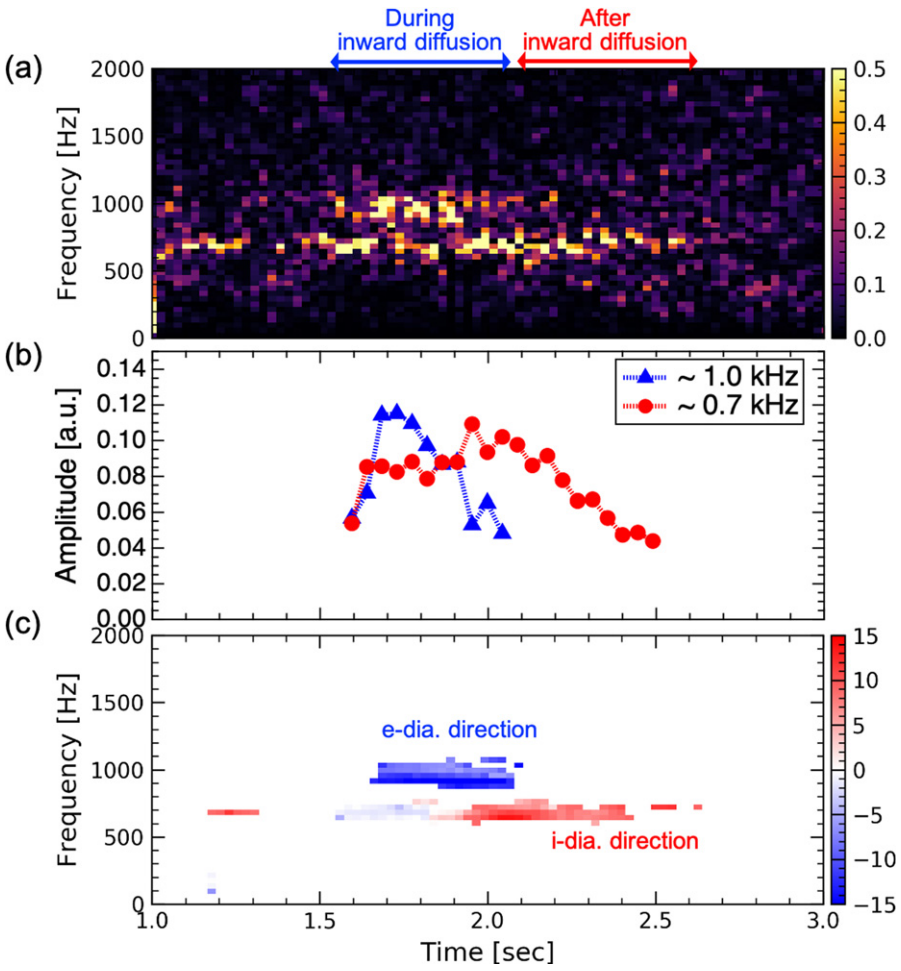

Figure 3. Time evolution of (*a*) the power spectral density of magnetic fluctuation, (*b*) the intensity of magnetic fluctuations for the 1 kHz and the 0.7 kHz components and (*c*) phase difference of two magnetic probes toroidally separated by $\Delta\varphi = 45$ degrees.

after the neutral-gas injection. The intensity of these magnetic fluctuations measured near the vacuum vessel is about 3% at 1 kHz component and about 4% at 0.7 kHz component of the equilibrium magnetic field (about 50 G) at the measurement position, respectively. The presence of such large magnetic fluctuations is considered to be a characteristic of high-beta plasmas. Figure 3(*b*) shows the time evolution of the intensity of each magnetic fluctuation component. During the inward diffusion, the fluctuation intensity of the 1 kHz component is dominant, while the intensity of the 0.7 kHz component is smaller than that of the 1 kHz component. After the inward diffusion, the fluctuation of the 1 kHz component decays, while the fluctuation of the 0.7 kHz component increases in intensity. This result shows a clear transition of the mode of fluctuations from the 1 kHz component to the 0.7 kHz component with the progress of the inward diffusion.

The profile of the fluctuation intensity of the line-averaged electron density was measured by a line-ratio spectroscopy. The fluctuation of the 1 kHz and the 0.7 kHz components were observed to be localized at $r < 0.7$ m and $r > 0.7$ m, respectively. Since the density peak which is formed by inward diffusion is about $r = 0.55$ m as in figure 2(*f*), the fluctuation of the 1 kHz component exists closer to the density peak than the 0.7 kHz component. The spatial propagation direction of the fluctuations is investigated using a magnetic probe array installed on the surface of the vacuum vessel of the RT-1. The typical phase velocities for the low-frequency fluctuations in toroidal and z-direction are 30 km s^{-1} ($k_\perp = 0.003$ cm^{-1}, $k_\perp \rho_\mathrm{i} \sim 0.02$) and 2 km s^{-1} ($k_\parallel = 0.02$ cm^{-1}, $k_\parallel \rho_\mathrm{i} \sim 0.2$), respectively. Here, the $k_\perp$ and $k_\parallel$ are wave number in the perpendicular and the parallel direction to the magnetic field, respectively, and the ρ_i is ion gyroradius. Figure 3(*c*) shows the time evolution of phase difference for each frequency component between two magnetic probes toroidally separated by $\Delta\varphi = 45$ degrees. In this figure, the waves with high correlation between the two measurement positions are extracted and displayed. During the inward diffusion from $t \sim 1.56$ s to $t \sim 2.1$ s, the fluctuation of the 1 kHz component propagates toroidally in the electron diamagnetic direction. After the inward diffusion, on the other hand, the fluctuation of the 1 kHz component disappeared and the fluctuation of the 0.7 kHz component which propagates in the ion diamagnetic direction is excited. The propagation direction and the intensity of the fluctuations depend on the density profiles, suggests that the drift wave instability is a possible candidate for the low-frequency fluctuations.

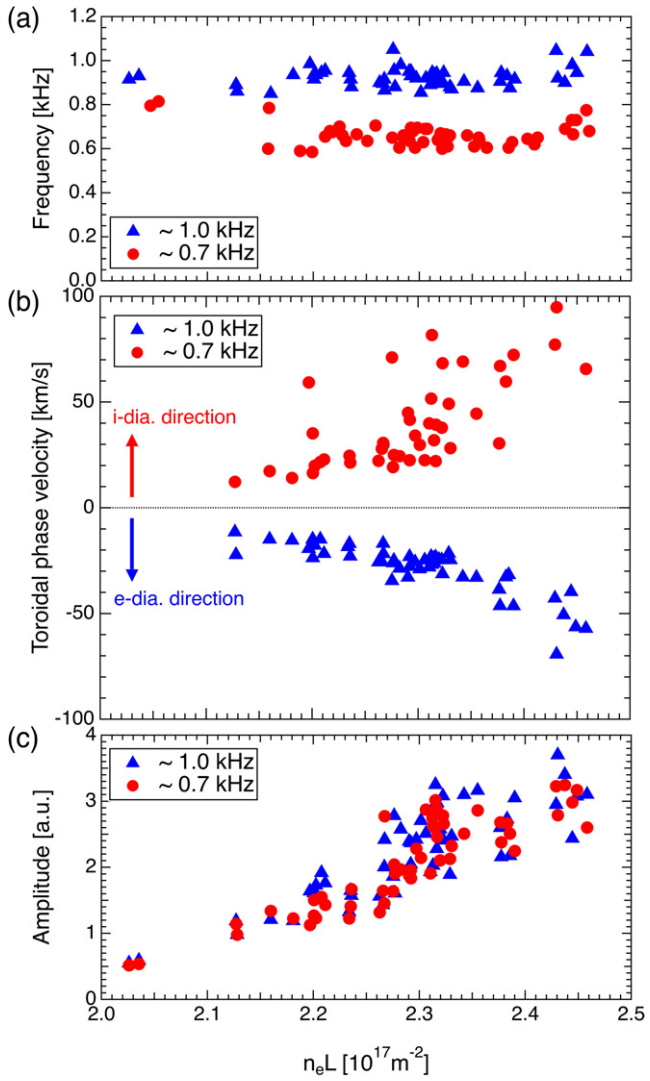

Figure 4. The line-integrated electron density dependence of (*a*) the frequency, (*b*) the toroidal phase velocity, and (*c*) the intensity of magnetic fluctuation for the 1 kHz (blue) and the 0.7 kHz (red) components.

The characteristics of each fluctuation component were investigated for various electron densities and plasma beta (or pressures). The frequencies of these low-frequency fluctuations are constant regardless of electron density and plasma beta (figure 4(*a*)). It was revealed that the phase velocity in the toroidal direction of the low-frequency fluctuations increases with an increase in the electron density (figure 4(*b*)); the fluctuation of the 1 kHz component increases from 10 to 60 km s^{-1} and the fluctuation of the 0.7 kHz component increases from 10 to 80 km s^{-1}, which were of the order of diamagnetic drift velocity of 10^4 m s^{-1} of the RT-1. Figures 4(*c*) and 5 show that the intensity of both fluctuations increase with the increase of line-averaged electron density and beta value, respectively. However, the intensity of both fluctuations strongly depends on the electron density rather than the plasma beta, suggesting that the 'free energy' causing the fluctuation is the distortion of the density profile.

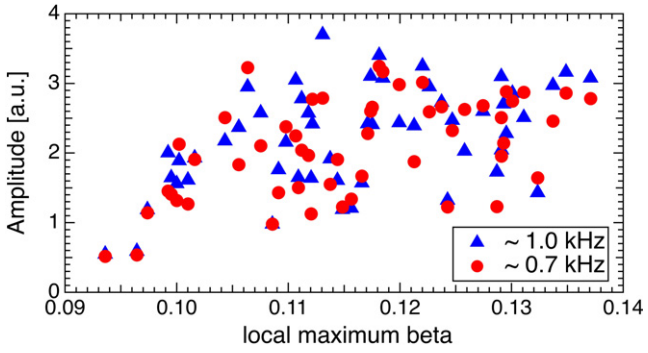

Figure 5. The β_e dependence of the intensity of magnetic fluctuations for the 1 kHz (blue) and the 0.7 kHz (red) components.

4. Discussion and summary

The low-frequency fluctuations observed in this study during the inward diffusion, considering the frequency range and phase velocity, are considered the transport of inhomogeneities frozen to the plasma flow. In particular, the density fluctuation caused by density inhomogeneities carried by the $\mathbf{E} \times \mathbf{B}$ drift transport, also reported as entropy mode in a dipole-confined plasma, is assumed to cause magnetic field fluctuations due to the high-beta condition in the RT-1. Here, low-frequency (<1 kHz) density fluctuations at the peripheral region are also observed in high-beta ($\beta > 1$) plasmas in the RT-1 [5], while they are considered to be a different mechanism from that observed during the inward diffusion in this study.

Similar phenomena have been observed in the CTX [12] and the LDX [8] as interchange and entropy modes. In the CTX, it has been reported that the instantaneous particle transport is intermittent, and the detailed time evolutions of the perturbed flux-tube number and potential indicate that convective transport dominates in the dipole configuration. In the LDX for dipole fueled pellet injection experiments, as the pellet passes through the plasma, it cools central electrons and creates a significant internal particle source. They have reported a reversal of the phase velocity for scrape-off-layer fluctuations.

In the RT-1, both the temperature and density profiles are thought to be flattened after the short period of neutral-gas injection, and we observed the dynamic change in density profile during the subsequent reconstruction with the inward diffusion. Although the shapes of the temperature and density profiles seem to be different between the RT-1 and the LDX, the directions of phase velocity of fluctuations are considered qualitatively consistent with that predicted by the entropy mode. On the other hand, the RT-1 shows a difference in the fluctuations of two frequency components rotating to electron and ion diamagnetic direction coexist at different radial positions during the inward diffusion. The mechanisms that determine the different directions of rotation and spatial structure of the fluctuations, and their relation to the diffusion direction, are the subject of future work.

The results are summarized as follows: (i) the self-organized peak density profile after the inward diffusion has been visualized by the tomography with deep learning technique; (ii) the existence of low-frequency fluctuations which drive inward diffusion has been experimentally proved and its physical characteristics have been revealed. These results advance our understanding of transport and self-organization not only in dipole plasmas, but also in general magnetic confinement systems relevant to fusion plasmas.

Acknowledgments

This work was supported by the NIFS Collaboration Research Program (Nos. NIFS15KOAH034 and NIFS19KBAR026), JSPS KAKENHI (Grant Nos. 17H01177, 18K13525 and 19KK0073) and 'PLADyS', JSPS Core-to-Core Program, A. Advanced Research Networks.

ORCID iDs

N. Kenmochi https://orcid.org/0000-0003-1088-8237
H. Saitoh https://orcid.org/0000-0001-8457-5570
Z. Yoshida https://orcid.org/0000-0002-9165-6616

References

[1] Yoshida Z. *et al* 2006 *Plasma Fusion Res.* **1** 008
[2] Yoshida Z., Saitoh H., Morikawa J., Yano Y., Watanabe S. and Ogawa Y. 2010 *Phys. Rev. Lett.* **104** 235004
[3] Yoshida Z. 2016 *Adv. Phys.:* X **1** 2
[4] Sato N. and Yoshida Z. 2018 *Phys. Rev.* E **97** 022145
[5] Nishiura M., Yoshida Z., Saitoh H., Yano Y., Kawazura Y., Nogami T., Yamasaki M., Mushiake T. and Kashyap A. 2015 *Nucl. Fusion* **55** 053019
[6] Nishiura M. *et al* 2017 *Nucl. Fusion* **57** 086038
[7] Boxer A.C., Bergmann R., Ellsworth J.L., Garnier D.T., Kesner J., Mauel M.E. and Woskov P. 2010 *Nat. Phys.* **6** 207
[8] Garnier D.T., Mauel M.E., Roberts T.M., Kesner J. and Woskov P.P. 2017 *Phys. Plasmas* **24** 012506
[9] Nishiura M., Yoshida Z., Kenmochi N., Sugata T., Nakamura K., Mori T., Katsura S., Shirahata K. and Howard J. 2019 *Nucl. Fusion* **59** 096005
[10] Kenmochi N., Nishiura M., Nakamura K. and Yoshida Z. 2019 *Plasma Fusion Res.* **14** 1202117
[11] Saitoh H., Yano Y., Yoshida Z., Nishiura M., Morikawa J., Kawazura Y., Nogami T. and Yamasaki M. 2015 *Phys. Plasmas* **22** 024503
[12] Grierson B.A., Mauel M.E., Worstell M.W. and Klassen M. 2010 *Phys. Rev. Lett.* **105** 205004